Coarsening in Polyethylene–Copolymer Blends

Buckley Crist* and Abhijit R. Nesarikar

Departments of Chemical Engineering and Materials Science and Engineering, Northwestern University, Evanston, Illinois 60208

Received August 15, 1994®

ABSTRACT: Artificially mixed binary blends of polyethylene and hydrogenated polybutadiene are equilibrated as two liquid phases at aging temperatures T_a = 140–160 °C. Phase separation occurs in ~30 s, followed by gradual coarsening of dispersed droplets during which the average particle size increases with time as $\bar{r}^3 \sim Kt$. The coarsening constant K is varied from 5×10^{-8} to 1.2×10^{-5} $\mu m^3/s$ by changing blend components and is compared to calculated rates based on coalescence and Ostwald ripening. Quantitative agreement is obtained for all conditions, even when the two coarsening mechanisms are operating in parallel with nearly equal rates. Coalescence is favored in blends with a low-viscosity matrix, while Ostwald ripening is dominant when both solubility and diffusivity of the minority component in the matrix are large.

Introduction

Polyethylene and its random copolymers provide extremely useful and important systems for the investigation of polymer–polymer blends. Studies in which both the strength of monomer–monomer interactions (the Flory–Huggins parameter χ) and the degree of polymerization are controlled have led to excellent understanding of thermodynamic behavior and the conditions under which one or two liquid phases are favored in binary systems.[1–7] These concepts have been extended to prediction of phase behavior in multicomponent systems such as linear low-density polyethylene.[8,9]

A more complicated issue is the manner in which a polymer–polymer liquid undergoes phase separation to achieve the equilibrium state. The vast majority of experimental and theoretical studies have addressed evolution of bicontinuous two-phase structures during spinodal decomposition, as reviewed recently by Hashimoto.[10] Phase separation may also occur by nucleation and growth of dispersed domains, though we are not aware of any systematic investigation of this process in polymers. Regardless of mechanism, liquid–liquid separation proceeds with substantial changes in phase concentrations and volume fractions as these quantities approach equilibrium values. The size scale within a phase-separated system depends on kinetic factors, though the process is driven by imbalance of "bulk" concentrations from equilibrium values. When true equilibrium is nearly attained, the excess free energy of the system is best expressed as an interfacial energy which may be reduced by decreasing the internal surface to volume ratio. Domain size thus increases by "coarsening" during which concentrations and volume fractions of the two phases are essentially constant, being imperceptibly displaced from the true equilibrium values which apply in the absence of interface effects. We are concerned here with coarsening that occurs over times many orders of magnitude larger than those required for phase separation.

Consider a binary system in which two liquid phases are stable. Liquid–liquid phase separation has occurred by either nucleation and growth or by spinodal decomposition to the point where volume fractions and concentrations of the two phases are at (or very near) their equilibrium values. Taking the usual case where one phase is dominant, one expects the two-phase liquid to have the minority phase (volume fraction f^β) dispersed as spherical particles in the continuous or matrix phase ($f^\alpha > f^\beta$). As mentioned above, the driving force for coarsening is reduction of internal surface or interfacial energy. Mechanisms most frequently considered for coarsening are coalescence and Ostwald ripening (also known as evaporation–condensation). Bicontinuous or "percolated" structures in critical systems may grow by viscous flow,[11,12] but that mechanism is not appropriate for the systems studied here.

The coalescence process, in which dispersed particles move through the matrix and collide with one another to form fewer, larger droplets, was the first to be analyzed. In the simplest treatment of Smoluchowski,[13,14] particle motion occurs by random Brownian motion in the matrix phase and only binary collisions are considered. During Ostwald ripening, on the other hand, smaller droplets dissolve and larger droplets grow; centers of mass of the particles are stationary, though "evaporation" will cause the smallest to disappear. This type of coarsening originates from concentration gradients in the matrix which are related to particle radius r.[15,16] For any value of the average matrix concentration C^α there are particles of a critical radius r_c which neither shrink nor grow because there is no local concentration gradient near such droplets. However, negative gradients exist near the interface of smaller particles ($r < r_c$) and positive gradients near larger particles ($r > r_c$), which lead to a net diffusive transfer from small to large droplets. Throughout this process, both the average radius $\bar{r}$ and critical radius r_c increase with time as the matrix concentration approaches its final equilibrium value C_e^α, which obtains in the absence of interface effects. It should be appreciated that changes in C^α and in f^β associated with Ostwald ripening are very small.

Both coalescence[14] and Ostwald ripening[17] have been reviewed adequately, though quantitative applications to polymer–polymer liquids are infrequent.[11,18,19] Important for any experimental study of coarsening is the same general time dependence for each mechanism:

$$\bar{r}^3 = \bar{r}_0^{\,3} + Kt \tag{1}$$

$$\frac{1}{N} = \frac{1}{N_0}\left[1 + \frac{Kt}{\bar{r}_0^{\,3}}\right] \tag{2}$$

The cube of the average particle radius $\bar{r}^3$ increases

® Abstract published in *Advance ACS Abstracts,* January 1, 1995.

0024-9297/95/2228-0890$09.00/0

linearly with time t, starting from the initial value $\bar{r}_0^3$ at time $t = 0$. Choice of the reference time $t = 0$ is arbitrary, provided liquid–liquid phase separation has been completed. K is the coarsening constant which depends on mechanism as well as temperature, volume fraction of dispersed phase f^β, etc. Equation 2 expresses the time dependence of N, the number density of particles. This expression follows from eq 1 and the definition of the mean particle volume $4\pi\bar{r}^3/3 \equiv f^\beta/N$. Implicit in eq 2 is the assumption that $g = \bar{r}^3/\bar{r}^3$, the ratio of the third moment of r to the cube of the first moment of r, is constant, a condition met for the self-similar particle size distributions obtained from asymptotic, long-time solutions for either Ostwald ripening[20] ($g = 1.18$ for $f^\beta \approx 0.15$) or coalescence[21] ($g = 1.59$). Evaluation of coarsening constant K is traditionally done in terms of eq 1 if Ostwald ripening is suspected, while eq 2 is employed for coalescing systems. However, either $\bar{r}^3(t)$ or $N^{-1}(t)$ can be used for either mechanism, or when both mechanisms operate simultaneously, with equal assurance. One final point is obvious, though worth stating; given that both coalescence and Ostwald ripening may occur in any liquid–liquid system, the identical time dependence of each means that there cannot be a "crossover" from one mechanism to the other with increasing time.

One usually does not know which coarsening mechanism is operative. With the reasonable assumption that Ostwald ripening and coalescence occur as independent, parallel processes, one can write

$$K = K_c + K_{OR} \tag{3}$$

The relative importance of the two terms in eq 3 can be found by evaluating them as follows:[20,21]

$$K_c = 2kTf^\beta/\pi\eta g \tag{4}$$

$$K_{OR} = (8D\nu_m\gamma C_e^\alpha/9kT)(1 + 0.74\sqrt{f^\beta})^3 \tag{5}$$

Brownian motion responsible for coalescence is expressed by the Stokes–Einstein diffusivity $D_p = kT/6\pi\eta r$ for a particle of radius r moving in a fluid of viscosity η under the influence of thermal energy kT. What enters in the expression for K_c is the product $D_p r$ which is independent of r, making the result in eq 4 independent of particle size and size distribution.[21] K_c thus depends only on temperature, matrix viscosity η, and the fraction of dispersed particles f^β. In this simplified form there is no energy barrier for coalescence, with each binary collision leading to the fusion of two particles. Equation 5 expresses the coarsening constant for Ostwald ripening in terms of the molecular diffusion coefficient D and equilibrium mole fraction C_e^α of blend components in the matrix (α) phase, molecular volume ν_m of the diffusing species, interfacial energy γ between the two coexisting phases, and thermal energy kT. The first factor is the classical result for vanishingly small dispersed phase fraction f^β. The second factor is the simplified result from Marqusee and Ross[20] to account for faster Ostwald ripening at finite phase fractions; it increases from 1.0 to 1.88 to 2.36 as f^β is increases incrementally from 0 to 0.1 to 0.2.

Calculation of K_{OR} for Ostwald ripening (eq 5) requires considerable knowledge about the binary system and its components. McMaster[11] studied the poly(acrylonitrile-*co*-styrene)/poly(methyl methacrylate) system in the first quantitative evaluation of coarsening in polymers. From the observed growth rate of dispersed droplets and the assumption that $K = K_{OR} \approx 10^{-6}$ $\mu m^3/s$, a reasonable estimate of the diffusion coefficient D was obtained. Mirabella has recently analyzed experimental coarsening rates for ethylene–propylene copolymer in polypropylene[18] and ethylene–butene copolymer in polyethylene[19] and found good agreement between experimental $K \approx 10^{-6}$ $\mu m^3/s$ and K_{OR} calculated from eq 5 (with $f^\beta = 0$). We are not aware of any prediction of coalescence rate for polymer–polymer liquids, even though particle motion has been observed in at least three sytems[10,22,23] and eq 4 requires only the matrix viscosity for evaluation. Parenthetically, we calculated K_c with eq 4 for Mirabella's polyethylene/copolymer blend[19] and found that coalescence is indeed negligible. Mirabella[18] had estimated "coalescence" rates based on sedimentation as opposed to Brownian motion; gravitational effects are not relevant to these systems.

Given that an experimental system coarsens with $\bar{r}^3 \propto t$, some alternatives to comparing observed and calculated rate constants are possible for establishing the mechanism. One method requires direct observation of particle motion, which is necessary, but not sufficient, for coalescence. One can also compare the experimental particle size distribution function to the positively skewed (coalescence[21]) or negatively skewed (Ostwald ripening[20]) distributions which are characteristic of the two mechanisms. It should be realized, however, that measurement of particle size distributions is an exacting exercise and that the theoretical distributions are rather variable.[24] A final method is to observe the dependence of K on volume fraction f^β, which is predicted to be linear for coalescence (eq 4) and more moderate for Ostwald ripening (eq 5).

We report experiments with phase-separated blends of nearly monodisperse polyethylene and hydrogenated polybutadiene, a model random copolymer of ethylene and butene-1. Thermodynamic and kinetic parameters are varied to alter the coarsening mechanism, and experimental rates are compared to theory. This is the first study that addresses quantitatively the coalescence rate in a polymer–polymer system.

Table 1. Chemical Characterization of Polymers

polymer	M_w (kg/mol)	M_w/M_n	y
PE32	32.1	1.11	0.0
PE120	119.6	1.19	0.0
HPB52	44.0	1.07	0.52
HPB58	50.2	1.11	0.58
HPB61	167	1.20	0.61

Experimental Section

Polymers and Blends. Two unbranched polyethylene (PE) fractions were purchased from the National Institute of Standards and Technology, and hydrogenated polybutadienes (HPB) were synthesized locally and characterized according to established procedures.[2,3,25] HPB is considered a random copolymer of linear and ethyl-branched C_4H_8 repeats with fraction y of ethyl-branched units, and PE is a homopolymer with $y = 0$. Polyethylenes are here labeled according to molecular weight while HPB*xx* has a suffix that is 100*y*; for example, PE32 is unbranched polymer with $M_w = 32.1$ kg/mol, and HPB61 is a branched polymer ($y = 0.61$). Chemical compositions and molecular weights are summarized in Table 1. It should be noted that the highly branched HPBs used in this work are completely amorphous at or above room temperature.

Blends were prepared by mixing PE and HPB at the desired ratio in boiling xylene, precipitating in a 5:1 excess of cold

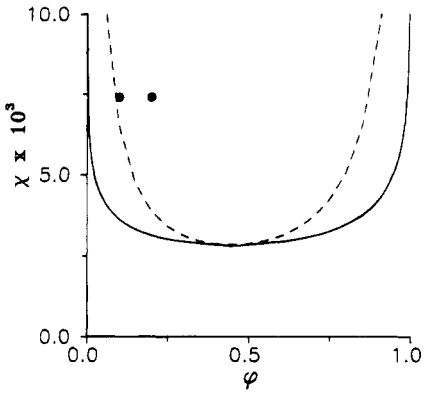

Figure 1. Phase diagram of PE32–HPB58 system at 150 °C. Solid line is the coexistence curve or binodal, dashed line is the spinodal, and points represent blends with composition φ = 0.1 and 0.2.

methanol containing the stabilizer Santanox (Montsanto Co.), and then drying under vacuum for ~1 h at room temperature. These artificially mixed systems are stable at room temperature because PE has crystallized, though they can phase separate, if thermodynamics in the liquid state so dictate, when heated above the melting point T_m = 135 °C of PE. Equilibrium liquid phase behavior was calculated with the Flory–Huggins interaction parameter for C_4H_8 repeat units in PE (y = 0) and HPB (y > 0) given by $\chi = 0.022y^2$ at 150 °C.[2,3] Binodals were evaluated by ignoring the modest polydispersity in molecular weights (Table 1). The phase diagram for a representative PE–HPB pair is presented in Figure 1, where two blends with different compositions are indicated by solid points. The volume fraction φ of HPB ranged from 0.10 to 0.20, chosen to give a reasonable amount of dispersed phase while avoiding theoretical complications present with large volume fractions of the coarsening particles. Five blends were prepared which are described by components and amount of HPB: PE32–HPB58-10, PE32–HPB58-20, PE32–HPB61-15, PE120–HPB61-15, and PE120–HPB52-10. For example, PE32–HPB58-10 is composed of the low molecular weight PE32 (M_w = 32.1 kg/mol, y = 0) blended with 10 wt % HPB58 (M_w = 50.2 kg/mol, y = 0.58). As melt densities of PE and HPB differ by less than 1%,[3] weight fraction equals volume fraction φ in the liquid state.

Coarsening Experiments. Figure 1 is typical of the phase relations in each blend system; all may be considered "deeply quenched" at or near 150 °C ($\chi \geq 2\chi_c$, where χ_c is the value of χ at the critical point) and have two equilibrium liquid phases. Similar to PE32–HBP58-20 (see Figure 1), blends PE32–HPB61-15 and PE120–HPB61-15 are in the unstable region of the phase diagram and are thus expected to demix by spinodal decomposition. PE32–HPB58-10 (see Figure 1) and PE120–HPB52-10 are both located very near the spinodal line. Since the rate of spinodal decomposition vanishes at the spinodal, liquid–liquid phase separation is most likely by nucleation and growth. The major phase (α) is nearly pure PE, which is expected to be continuous and should crystallize readily when the melt is cooled below 120 °C, while the minor phase (β) of dispersed HPB-rich droplets will remain amorphous. Quantitative calculations of binodals for the systems used here show the maximum solubility (volume fraction) of HPB in the matrix phase ϕ_e^{α} and the maximum solubility of PE in the dispersed phase $(1 - \phi_e^{\beta})$ to be less than 6×10^{-3}. The near purity of the two liquid phases is used later when coarsening constants are calculated. It is assumed that temperature changes between 140 and 160 °C have no effect on equilibrium phase behavior.

Some experiments were done with optical microscopic observation of coarsening at an aging temperature T_a = 140 °C on 5–10 μm thick films in a Mettler hot stage with nitrogen purge. Optical contrast was very weak in the liquid state, though it was possible to resolve fairly large spherical dispersed domains (HPB droplets) which were unchanged by cooling to crystallize the PE matrix. Under crossed polarizers, the distinction between amorphous HPB droplets and birefringent, crystallized PE matrix was excellent at temperatures less than 110 °C. Nevertheless, submicrometer-sized particles are not detected with optical microscopy, meaning that the correct average droplet radius $\bar{r}$ could not be obtained and that the apparent volume fraction of dispersed particles, f^{β}, was about one-third of its expected value, even after 10 h of aging. Other complications stem from stereological issues and the possibility of two-dimensional growth in thin films. For these reasons, optical microscopy was used for qualitative purposes only. Beyond establishing that crystallization indeed traps the morphology of the liquid, this method permits observation of a single volume element as a function of time.

Quantitative studies were done on samples prepared as follows. Dried powder was compression molded in a heated press at an aging temperature T_a between 140 and 160 °C for $t \approx 30$ s and then quench crystallized in cold water. A small portion of the film of ~300 μm thickness was examined for phase separation as described below. The balance was returned to the press, heated for longer aging times (up to t = 125 min or 7500 s), and then quenched and a section removed after each time increment. Certain blends with sluggish coarsening kinetics required aging times up to 600 min; these were heated in a vacuum oven to minimize oxidation. With this procedure, different portions of a single sample could be investigated as a function of aging time t. Nevertheless, heterogeneity of the melt structure may cause sampling errors when different limited regions are analyzed at distinct times.

Quench-crystallized samples were ultramicrotomed at −120 °C to expose an internal surface. As the two phases are nearly pure PE and HPB, selective etching to remove amorphous polymer serves to define the phase structure in the melt. Following Mirabella et al.[19,26] we used n-heptane in an ultrasonic bath for 30 min at 55 °C. Microtomed and etched surfaces were coated with gold and examined in a Hitachi S-510 scanning electron microscope (SEM). What had been dispersed HPB domains are seen as roughly circular cavities in the otherwise continuous PE matrix. Representative micrographs of a blend at short and long coarsening times are shown in Figure 2. It is assumed here that the quench-crystallized, microtomed, and etched morphology gives an accurate image of the phase-separated liquid. Different thermal contractions of crystallizable PE matrix and amorphous HPB droplets are ignored.

Stereology. The two-dimensional sections of phase-separated "frozen liquid" were analyzed as follows. A test area A (30–1000 μm^2, depending on coarsening time) incorporating 100–300 particles was selected. The diameter of each particle cross section (which is a chord, not the diameter, of the spherical droplet) was defined by a pair of x–y coordinates established visually and entered into a data file with a digitizer (Houston Instruments). An effective diameter was estimated for droplets with noncircular sections. The data set of the number of particles N_i and corresponding chord length ξ_i was used to evaluate the average particle radius $\bar{r}$ and the volume fraction f^{β} of the dispersed phase:[27,28]

$$\bar{r} = \frac{\pi}{4}\frac{\sum N_i}{\sum(N_i/\xi_i)} \tag{6}$$

$$f^{\beta} = \frac{\pi}{4A}\sum \xi_i^2 N_i \tag{7}$$

Here N_i is a pure number, not to be confused with the number density N in eq 2 or the degree of polymerization in eq 8 below.

Analysis and Results

SEM photographs such as Figure 2 clearly show that the two-phase liquid morphology has evolved from the artificially mixed state after t = 60 s in the melt and that the nearly spherical particles increase in size and decrease in number as aging time increases. Coarsening data were plotted as $\bar{r}^3$ (from eq 6) vs time t. Here

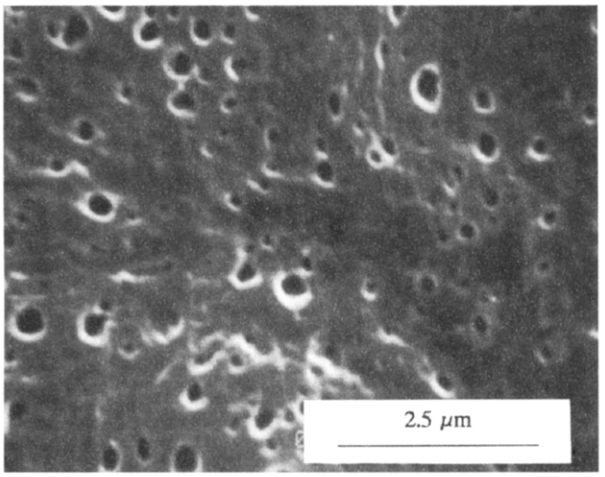

(a)

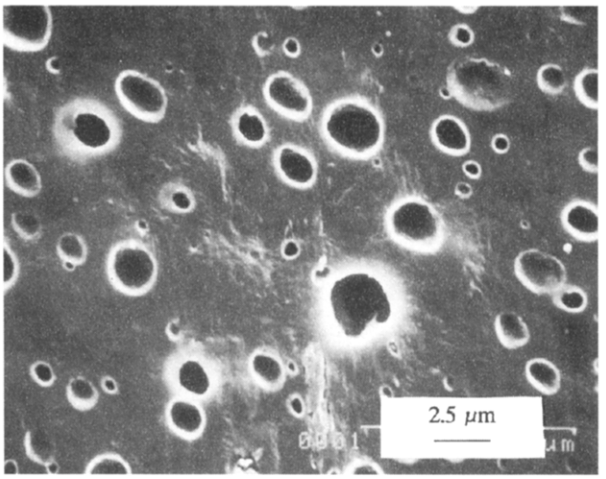

(b)

Figure 2. Micrographs of microtomed and etched surfaces of PE120–HPB52-10 blend after aging at 160 °C for (a) 1 and (b) 125 min. Note lower magnification in (b).

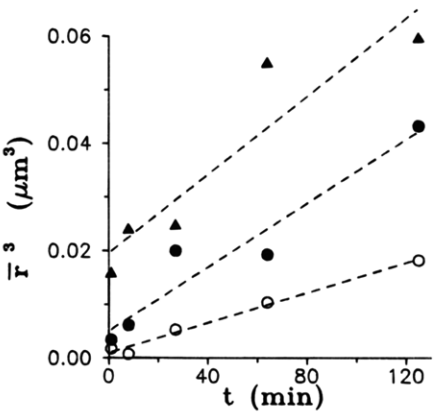

Figure 3. Cube of average particle radius as a function of aging time for PE32–HPB58-10 at 140 °C (○), PE32–HPB58-10 at 160 °C (●), and PE32–HPB58-20 at 160 °C (▲).

t is the total time in the melt, but correction for the ~10 s required for phase separation is insignificant. Representative results for PE32–HPB58 blends in Figure 3 are linear, in accord with eq 1, the slope giving the coarsening constant K. Deviations from strictly linear behavior are attributed to sampling errors mentioned earlier. It appears that K increases with aging temperature T_a and that the volume fraction of dispersed phase f^β has a small effect. One comment is in order regarding the format of Figure 3. One often sees plots of log $\bar{r}$ vs log t,[11,18,19,22,23] which are sensible provided that $\bar{r}_0^3 \ll Kt$. This is clearly not the case for PE32–HPB58-20 in Figure 3, where a log–log plot would be distinctly concave upward because of the large value of $\bar{r}_0^3$, obscuring the fact that $\bar{r}^3 \propto t$.

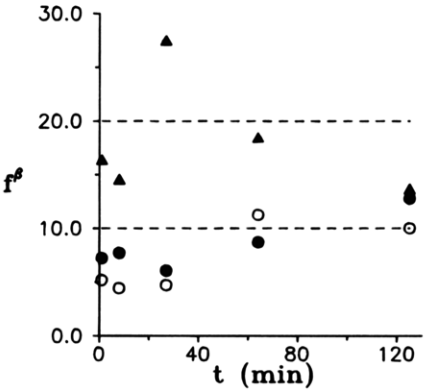

Figure 4. Dispersed phase volume fraction f^β calculated from eq 7 as a function of aging time for PE32–HPB58-10 at 140 °C (○), PE32–HPB58-10 at 160 °C (●), and PE32–HPB58-20 at 160 °C (▲).

As coarsening by either Ostwald ripening or coalescence is presumed to occur at constant (or nearly constant) phase fraction f^β, this quantity was evaluated from the stereology data by eq 7 and plotted in Figure 4. Experimental points conform reasonably well to the expected values $f^\beta = \varphi$ (phases are essentially pure PE and HPB as mentioned earlier) represented by horizontal dashed lines. Data for PE32–HPB58-20 suggest sampling error fluctuations of ±0.05 (±25%) about a time-independent $f^\beta = 0.20$. For PE32–HPB58-10, f^β appears systematically less than $\varphi = 0.10$ for $t < 60$ min. It is possible that phase separation is not complete (i.e., equilibrium compositions and volume fractions of the two liquid phases have not been achieved) until ~60 min has passed, though we believe it is more likely that the smallest particles are missed in the analysis, leading to an underestimation of f^β, or that sampling errors at least contribute to the discrepancy. There is no correlation between fluctuations in coarsening data in Figure 3 and in volume fraction data in Figure 4. Volume fractions were not considered in other treatments of coarsening in polymer systems of which we are aware.

These experiments indicate that $\bar{r}^3 \sim Kt$ over the time scale of 1–600 min for the PE–HPB blends studied here. As experimental $f^\beta \approx \varphi$ over the same times, there is no indication of "pinning" the liquid–liquid phase separation process in off-critical blends as reported by Hashimoto et al.[29] One feature observed in the present work is related to that concept, however. Notice in Figure 3 that $\bar{r}_0^3$ is much larger for PE32–HPB-20 than for PE32–HPB-10. From Figure 1, the $\varphi = 0.2$ blend is clearly unstable and phase separates by spinodal decomposition, first forming a bicontinuous structure which "pinches off" into droplets (percolation to cluster transition).[2,29] The $\varphi = 0.1$ blend is located nearly on the spinodal line where the rate of spinodal decomposition approaches 0; hence it probably phase separates by nucleation and growth. Thus we observe that a higher volume fraction of the minority phase (or deeper quench) leads to larger particles being formed during liquid–liquid phase separation, in qualitative accord with Hashimoto et al.[29] The same correlation between

Table 2. Experimental and Theoretical Coarsening Constants

blend	T_a (°C)	K (10^{-6} μm^3 s^{-1})	$K_c + K_{OR}$ (10^{-6} μm^3 s^{-1})	K_c (10^{-6} μm^3 s^{-1})	η (10^3 P)	K_{OR} (10^{-6} μm^3 s^{-1})	C_e^α	D (10^{-10} cm^2 s^{-1})
PE120–HPB61-15	150	0.049	0.021	0.021	168	6.4×10^{-8}	2.67×10^{-10}	0.16
PE32–HPB61-15	150	4.2 ± 1	2.2	2.2	1.65	7.7×10^{-8}	3.20×10^{-10}	0.16
PE32–HPB58-10	140	2.2	2.1	1.2	2.01	0.86	1.54×10^{-3}	1.4
PE32–HPB58-10	160	4.9 ± 1	3.4	1.5	1.65	1.9	1.54×10^{-3}	3.1
PE32–HPB58-20	160	6.0 ± 2	5.4	3.0	1.65	2.4	1.54×10^{-3}	3.1
PE120–HPB52-10	160	10.2	10.8	0.017	140	10.8	1.58×10^{-2}	2.2

$\bar{r}_0^3$ and demixing process was seen in PE120–HPB52 (metastable, nucleation, and growth, small $\bar{r}_0^3$) and PE32–HPB61 (unstable, spinodal decomposition, large $\bar{r}_0^3$).

Discussion

Coarsening constants K for the six experiments are presented in Table 2. Where no error limits are indicated, scatter in $\bar{r}^3$ vs t data corresponds to an uncertainty in K of less than ±15%. Also in the table are the sum $K_c + K_{OR}$ (eq 3), the individual terms K_c and K_{OR} evaluated by eqs 4 and 5, respectively, and some of the parameters used in the calculations. Row order conforms generally to increasing importance of Ostwald ripening; PE120–HPB61-15 at the top is dominated by coalescence, while PE120–HPB52-10 at the bottom coarsens by Ostwald ripening. Experimental coarsening constants and the calculated rates $K_c + K_{OR}$ are in the range of 10^{-8}–10^{-5} $\mu m^3/s$. Before discussing the relation between observed and theoretical values, some consideration should be given to the calculations.

K_c as expressed by eq 4 requires only matrix viscosity η, which was measured by Raju et al.[30] for the two polyethylene reference materials used in this work, and is entered in Table 2. The matrix phase is treated as pure PE, as justified from binodals mentioned earlier which indicate that $\phi_e^\alpha < 6 \times 10^{-3}$. Changing the matrix from PE120 to PE32 decreases η by 100-fold and increases the coalescence rate by the same factor (from $\sim 10^{-8}$ to $\sim 10^{-6}$ $\mu m^3/s$).

Of the parameters in eq 5 for K_{OR}, only the mole fraction of HPB in the matrix, C_e^α, derived directly from equilibrium volume fraction ϕ_e^α, depends strongly on phase concentrations. Notice in Table 2 that C_e^α increases from $\sim 10^{-10}$, for blends using the highest molecular weight and most branched HPB61, to $\sim 10^{-2}$ for PE120–HPB52, which has the least "deep" quench because of relatively low M_w and y of the HPB component. Ostwald ripening requires mutual diffusion of HPB and PE through the matrix (α) phase which is described by[31]

$$D = [(1 - \phi_e^\alpha)N_{HPB}D_{HPB} + \phi_e^\alpha N_{PE}D_{PE}][(1 - \phi_e^\alpha)/N_{HPB} + \phi_e^\alpha/N_{PE} - 2\chi\phi_e^\alpha(1 - \phi_e^\alpha)] \quad (8)$$

Here D_j is the diffusion coefficient and N_j is the degree of polymerization, based on C_4H_8 units, for HPB or PE. Since the matrix phase is nearly pure PE and its concentration is far from the spinodal, one can anticipate that $D \approx D_{HPB}$. For the diffusivity of unbranched PE, we use the experimental results of Klein and Briscoe.[32] More important is D_{HPB}, which should correspond to the tracer diffusion coefficient of HPB in the PE matrix at the aging temperature T_a. No data are available, so we make the logical assumption that tracer diffusivity is controlled by matrix dynamics and the length of the reptating diffusant[33] and employ self-diffusion coefficients of unbranched PE having the same chain length as HPB. D calculated by eq 8, which is within 10% of D_{HPB}, increases by a factor of ~20 as HPB chain length is reduced on going from the top to the bottom of Table 2. Also required in eq 5 are molecular volume v_m for the HPB component ($(9.1–34.6) \times 10^{-20}$ cm^3 in these systems) and surface energy $\gamma = 1.19–1.37$ erg/cm^2 calculated from Helfand and Sapse[34] by assuming "pure phases" $\phi_e^\alpha = 0$ with segment lengths measured by neutron scattering.[35]

In Table 2 it is seen that measured and calculated coarsening constants track one another over the 250-fold range of the present results. Individual terms in the theoretical rate $K_c + K_{OR}$ permit interpretation of the observed behavior, which falls into three categories. PE120–HPB61-15 and PE32–HPB61-15 comprise the first group which coarsens exclusively by coalescence ($K_c \gg K_{OR}$). These two blends differ in molecular weight of the PE matrix, causing the change in $K = K_c$ through matrix viscosity as mentioned above. Ostwald ripening is extremely slow ($K_{OR} < 10^{-13}$ $\mu m^3/s$) because of the high molecular weight of the HPB component. Inspection of eq 5 leads to the prediction that increased HPB molecular weight will cause D and hence K_{OR} to decrease. This is true, but not the major effect; the matrix solubility C_e^α of HPB61 is orders of magnitude smaller than for other groups. High molecular weight and branching (see Table 1) both contribute to a large "quench depth" with low solubility which suppresses Ostwald ripening.

The second group of blends is PE32–HPB58-10 and PE32–HPB58-20, for which K_c and K_{OR} are comparable in magnitude. Coalescence is essentially the same as for PE32–HPB61-10 in the previous group, since the PE component (viscosity η) is unchanged. Ostwald ripening has been enhanced substantially, mainly through increased solubility C_e^α achieved by lowering M_w and y of the HPB component. Effects of temperature and blend composition are seen to follow, at least qualitatively, the trends predicted by theory. A 20 °C temperature rise more than doubles K, while the calculated rate $K_c + K_{OR}$ increases by 70%. Increasing the dispersed phase fraction f^β from 0.1 to 0.2 likewise increases K, though only by 20% as opposed to the calculated change of 60%. These discrepancies are acceptable, given the experimental uncertainty in K and the assumption of strict additivity of rates in eq 3.

PE120–HPB52, which coarsens by Ostwald ripening, constitutes the last blend type. Coalescence is slowed by high matrix molecular weight, while Ostwald ripening is favored by HPB with the lowest M_w and y, increasing both D and C_e^α.

Agreement between experimental and theoretical coarsening constants for coalescence only (PE120–HPB61-15 and PE32–HPB61-15), "mixed" coalescence and Ostwald ripening (PE32–HPB58), and Ostwald ripening only (PE120–HPB52-10) is gratifying. For the latter blend, nearly perfect accord between K and K_{OR} may be fortuitous. Calculated constants $K_c + K_{OR}$ are, however, sometimes lower than the observed K for the

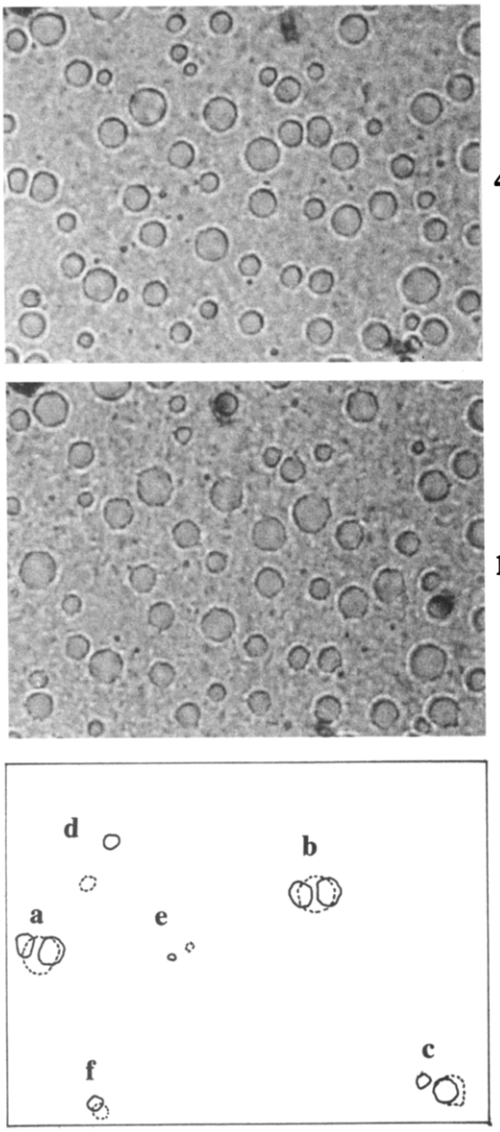

Figure 5. Optical micrographs (full width is 100 μm) of PE32–HPB58-20 coarsening at 140 °C for the indicated times. The sketch indicates examples of particle fusion (a–c) and particle motion (d–f).

other systems in which coalescence is dominant or significant. The entries in Table 2 indicate that K_c from eq 4 is about half the experimental coalescence rate, though the cause of this rather modest difference is not known. It may be some uncontrolled aspect of the experiment or polymer characterization. Another possibility is enhancement of the coalescence rate by something like "collision-induced collision" proposed by Tanaka.[23] We evaluated $K = 2.7 \times 10^{-2}$ μm^3/s from Tanaka's data for oligomeric styrene and caprolactam and find that it is also ~2 times larger than the classical K_c given by eq 4. This may be a coincidence, but it provides another indication that the Smoluchowski model may underestimate coarsening in polymer liquids.

We conclude this section with a brief presentation of evidence for coalescence from optical micrographs in Figure 5. The blend is PE32–HPB58-20 at 140 °C imaged after 450 and 1200 min; adventitious dirt particles ensure that the same area is being observed. From Table 2 it is predicted that $K_c \approx K_{OR}$, i.e., that coalescence and Ostwald ripening make similar contributions to K. Coalescence is consistent with both fusion of adjacent droplets (a–c) and particle motion (e–f) which occur over the 750 min time interval; examples are sketched in the cartoon accompanying the micrographs. It should be re-emphasized, however, that such "direct" observation of particle dynamics does not establish coalescence as the dominant coarsening mechanism. Droplet motion and fusion will always occur in liquid–liquid systems over suitable time scales, though it is possible that Ostwald ripening is the faster mechanism. The converse is probably true; if no evidence is found for particle motion while $\bar{r}^3$ increases appreciably, Ostwald ripening is almost certainly dominant.

Conclusions

This is the first study of coarsening in polymer liquids that considers both coalescence and Ostwald ripening. Blends based on well-characterized and nearly monodisperse components permit definitive comparison of theory to experiment. The growth of dispersed domains in phase-separated liquids of polyethylene and model copolymers follows the classical expectation $\bar{r}^3 \sim Kt$ for coarsening. The coarsening mechanism can be shifted from coalescence to Ostwald ripening by controlling blend components and overall composition φ. Good agreement is obtained between experimental and calculated coarsening constants, even when both mechanisms are contributing to the observed rate. This indicates that the parallel process assumption implicit in eq 3, i.e., that neither mechanism is substantially modified by the presence of the other, is reasonable.

Coalescence rate K_c is manipulated in a straightforward manner through viscosity $\eta \propto M_w^{3.4}$ of the matrix phase. Ostwald ripening is more subtle, K_{OR} being dependent on both diffusivity D and solubility C_e^{α} of the minority component (HPB in the present study) in the matrix phase. To a good approximation, $D \propto M_w^{-2}$ for the HPB, but molecular weight changes have an even larger effect (in the same direction) on C_e^{α}. Solubility C_e^{α} may be changed independently of D through $\chi \propto y^2$ of the HPB component. K_{OR} also depends on interfacial energy $\gamma \propto \chi^{1/2}$, but this is typically about 1 erg/cm^2 in phase-separated blends of high molecular weight polymers at conventional temperatures. In summary, coalescence is favored in blends with relatively fluid matrices at large quench depths, while Ostwald ripening is observed when shallow quenches and large molecular weight matrices are employed.

The principles outlined here should apply directly to other polymer–polymer systems. Multicomponent blends may prove to be interesting, if challenging, subjects of future study. Park and Roe[36] have observed K to decrease in the presence of a block copolymer, presumably through lowering interfacial energy γ, which drives Ostwald ripening. This effect should vanish in a comparable ternary system undergoing coalescence, provided the assumption of negligible energy barrier for particle fusion, implicit in eq 4 and demonstrated here, still holds. More pertinent to the present work are commercial materials such as linear low-density polyethylene, a complex multicomponent copolymer that exhibits two liquid phases.[9] These systems have been observed to coarsen,[37] and comparison to suitable theory would be of considerable scientific and technological interest.

Acknowledgment. This work was supported by the David and Lucile Packard Foundation through a fellowship awarded to Professor Olvera de la Cruz and by

the Exxon Educational Foundation. We are indebted to Dana Underwood, a participant in Northwestern's Materials Research Internship for Minority Undergraduates program funded by the National Science Foundation, for experimental assistance. Peter Voorhees, Julio Ottino, Monica Olvera, and William Graessley are thanked for helpful discussions.

References and Notes

(1) Nicholson, J. C.; Finerman, T. M.; Crist, B. *Polymer* **1990**, *31*, 2287.
(2) Rhee, J.; Crist, B. *Macromolecules* **1991**, *24*, 5663.
(3) Rhee, J.; Crist, B. *J. Chem. Phys.* **1993**, *98*, 4174.
(4) Balsara, N. P.; Fetters, L. J.; Hadjichristidis, N.; Lohse, D. J.; Han, C. C.; Graessley, W. W.; Krishnamoorti, R. *Macromolecules* **1992**, *25*, 6137.
(5) Budkowski, A.; Klein, J.; Eisner, E.; Steiner, U.; Fetters, L. J. *Macromolecules* **1993**, *26*, 3858.
(6) Alamo, R. G.; Londono, J. D.; Mandelkern, L.; Stehling, F. C.; Wignall, G. D. *Macromolecules* **1994**, *27*, 411.
(7) Krishnamoorti, R.; Graessley, W. W.; Balsara, N.; Lohse, D. *J. Chem. Phys.* **1994**, *100*, 3894.
(8) Nesarikar, A.; Olvera de la Cruz, M.; Crist, B. *J. Chem. Phys.* **1993**, *98*, 7385.
(9) Nesarikar, A.; Crist, B.; Davidovich, A. *J. Polym. Sci., Part B: Polym. Phys. Ed.* **1994**, *32*, 641.
(10) Hashimoto, T. In *Materials Science and Technology*; Thomas, E. L., Ed.; VCH: New York, 1993; Vol. 12, pp 251–300.
(11) McMaster, L. P. *Adv. Chem. Ser.* **1975**, *No. 142*, 43.
(12) Siggia, E. D. *Phys. Rev. A* **1979**, *20*, 595.
(13) von Smoluchowski, M. *Phys. Z.* **1916**, *17*, 557, 585.
(14) Levich, V. G. *Physicochemical Hydrodynamics*; Prentice-Hall: Englewood Cliffs, NJ, 1962; pp 207–211.
(15) Lifshitz, I. M.; Slyozov, V. V. *J. Phys. Chem. Solids* **1961**, *19*, 35.
(16) Wagner, C. *Z. Elektrochemie* **1961**, *65*, 581.
(17) Voorhees, P. W. *Annu. Rev. Mater. Sci.* **1992**, *22*, 197.
(18) Mirabella, F. M. *J. Polym. Sci., Part B: Polym. Phys. Ed.* **1994**, *32*, 1205.
(19) Mirabella, F. M.; Barley, J. S. *J. Polym. Sci., Part B: Polym. Phys. Ed.* **1994**, *32*, 2187.
(20) Marqusee, J. A.; Ross, J. *J. Chem. Phys.* **1984**, *80*, 536.
(21) Friedlander, S. K. *Smoke, Dust and Haze*; Wiley: New York, 1977; pp 175–200.
(22) Jang, B. Z.; Uhlmann, D. R.; Vander Sande, J. B. *Rubber Chem. Tech.* **1984**, *57*, 291.
(23) Tanaka, H. *Phys. Rev. Lett.* **1994**, *72*, 1702.
(24) Chen, M. K.; Voorhees, P. W. *Modelling Simul. Mater. Sci. Eng.* **1993**, *1*, 591.
(25) Krigas, T. M.; Carella, J. M.; Struglinski, M. J.; Crist, B.; Graessley, W. W.; Schilling, F. C. *J. Polym. Sci., Part B: Polym. Phys. Ed.* **1985**, *23*, 509.
(26) Mirabella, F. M.; Westphal, S. P.; Fernando, P. L.; Ford, E. A.; Williams, J. G. *J. Polym. Sci., Part B: Polym. Phys. Ed.* **1988**, *26*, 1995.
(27) Fullman, R. L. *Trans. Am. Inst. Min., Metall. Pet. Eng.* **1953**, *197*, 447.
(28) Underwood, E. E. *Quantitative Stereology*; Addison-Wesley: Menlo Park, CA, 1970; pp 81 ff.
(29) Hashimoto, T.; Takenaka, M.; Izumitani, T. *J. Chem. Phys.* **1992**, *97*, 679.
(30) Raju, V. R.; Smith, G. G.; Marin, G.; Knox, J. R.; Graessley, W. W. *J. Polym. Sci., Polym. Phys. Ed.* **1979**, *17*, 1183.
(31) Composto, R. J.; Kramer, E. J.; White, D. M. *Nature* **1987**, *328*, 234.
(32) Klein, J.; Briscoe, B. J. *Proc. R. Soc. London, Ser. A* **1979**, *365*, 53.
(33) Graessley, W. W., personal communication.
(34) Helfand, E.; Sapse, A. M. *J. Chem. Phys.* **1975**, *62*, 1327.
(35) Rhee, J. Ph.D. Thesis, Northwestern University, Evanston, IL, 1992.
(36) Park, D. W.; Roe, R. J. *Macromolecules* **1991**, *24*, 5324.
(37) Mirabella, F. M., personal communication.

MA9411383